Supporting Information

A Fluorescent Hydrogen-Bonded Organic Framework for Highly Selective Sensing of Mono-Nitrophenol Isomers in Water

Yu-Xin Lin,‡ Chenghao Jiang,‡ Yu-Bo Wang,‡ Jia-Xin Wang, Bin Li* and Guodong Qian*

State Key Laboratory of Silicon and Advanced Semiconductor Materials, School of Materials Science and Engineering, Zhejiang University, Hangzhou, 310027, China.

**Corresponding author: Email: bin.li@zju.edu.cn; gdqian@zju.edu.cn.*

‡ These authors have contributed equally to this work.

Configurational Bias Monte Carlo (CBMC) simulation

In order to obtain a reasonable binding site of PNP molecules in HOF-TPE-CN for subsequent modeling, configurational-bias Monte Carlo (CBMC) simulations were performed in the MS modeling.[1,2] The structure of HOF-TPE-CN, obtained from the single crystal structure without further geometry optimization, was assumed to be rigid according to the atom crystallographic positions. The structural file of PNP was taken from Chem 3D with minimum energy optimization. The calculations were performed at 298 K, adopting the universal force field (UFF) combined with the QEq method. Interatomic interactions were modeled with standard Lennard-Jones potential and Coulombic potentials. The long-range electrostatic interactions were handled using the Ewald summation method. The loading steps and the equilibration steps were 1×10^5, the production steps were 1×10^6. A nonbonding parameter was utilized to determine the pairwise interactions between the host and guest atoms of the particular force field.

Density functional theory calculations

The calculated structure of HOF-TPE-CN was built from its single crystal structures and the position of the hydrogen atom was optimized while the other atoms kept their position unchanged. The long-range corrected hybrid functional CAM-B3lyp was carried out with the 6-311G(d) basis set for ONP, MNP, PNP, and the fragment of HOF.[3] The DFT-D3 with BJ-damping was applied to correct the weak interaction to improve the calculation accuracy. Calculations are then performed to determine orbital energy levels and to analyze orbital diagrams.

Calculations of K_{sv} and detection limit

Quenching constant K_{sv} was calculated according to the Stein–Volmer (S–V) equation:[4]

$$I_0/I - 1 = K_{sv}\,[A] \qquad (2)$$

where I_0 and I represent the fluorescence intensities of HOF-TPE-CN probes before and after the addition of nitrophenols, respectively. [A] is the molar concentration of nitrophenols. There is a linear relationship between [A] and I_0/I at low concentrations. K_{sv} was obtained by plotting the change in the fluorescence intensity *vs* the concentration of nitrophenols.

The limit of detection was calculated based on the IUPAC recommendation ($3\sigma/K$) method. The standard deviation σ was estimated by the fluorescence intensity of the 10 blank HOF-TPE-CN/water suspension in the absence of analytes. K is the slope value of the linearity, which is calculated using a calibration curve for the fluorescence intensity *vs* the concentration of nitrophenols.

General characterization

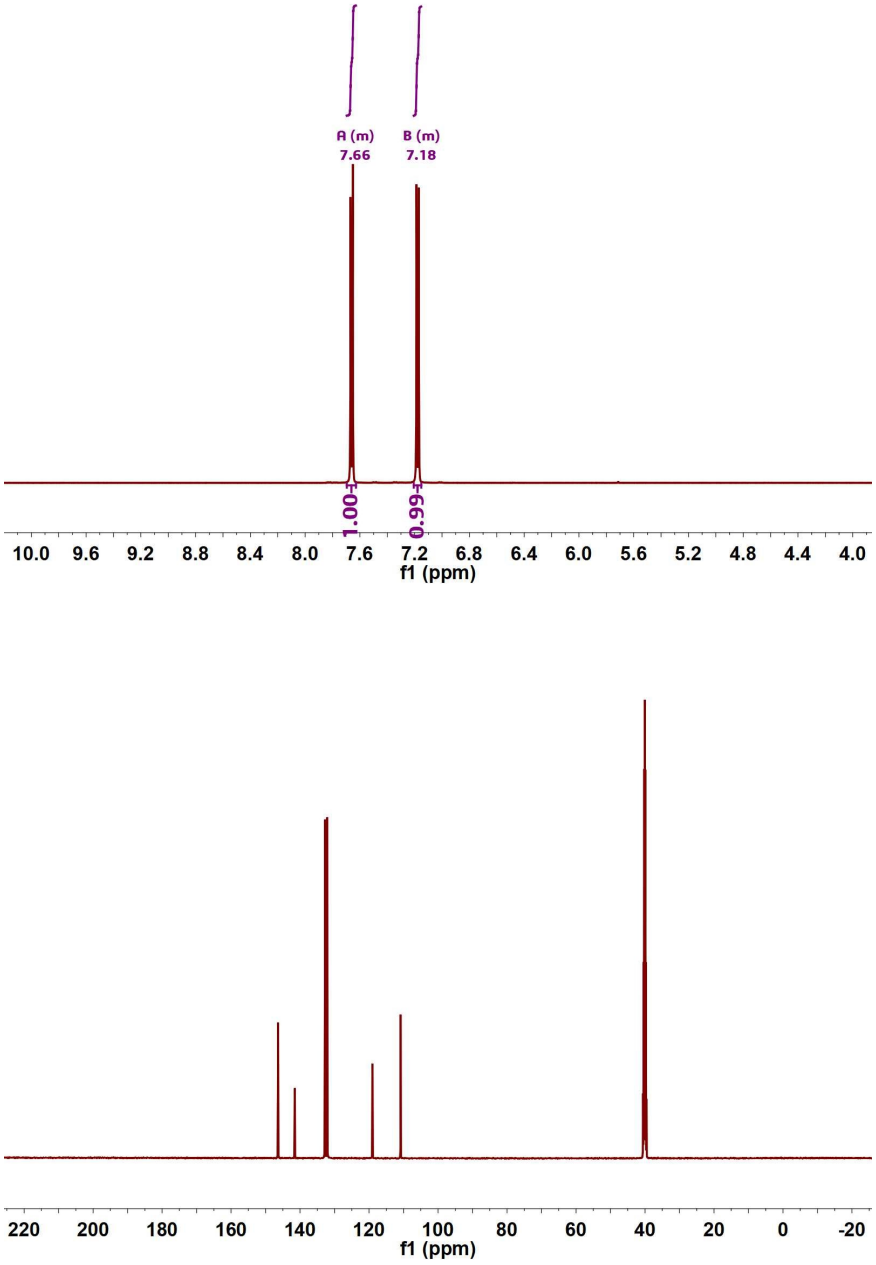

Fig. S1 ^{1}H NMR and ^{13}C NMR spectrum of TPE-CN in DMSO-d_6.

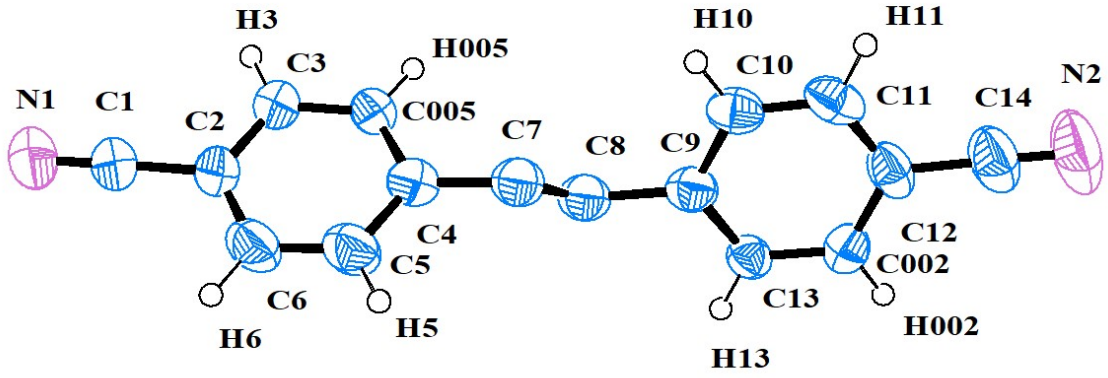

Fig. S2 ORTEP plot of the asymmetric unit of HOF-TPE-CN.[5] All non-hydrogen atoms are represented by thermal ellipsoids drawn at 50% probability level.

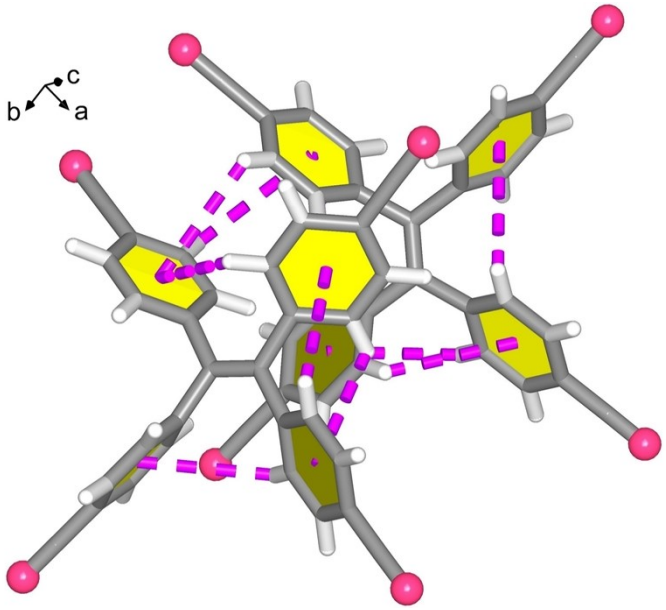

Fig. S3 Peripheral C–H···π interactions.

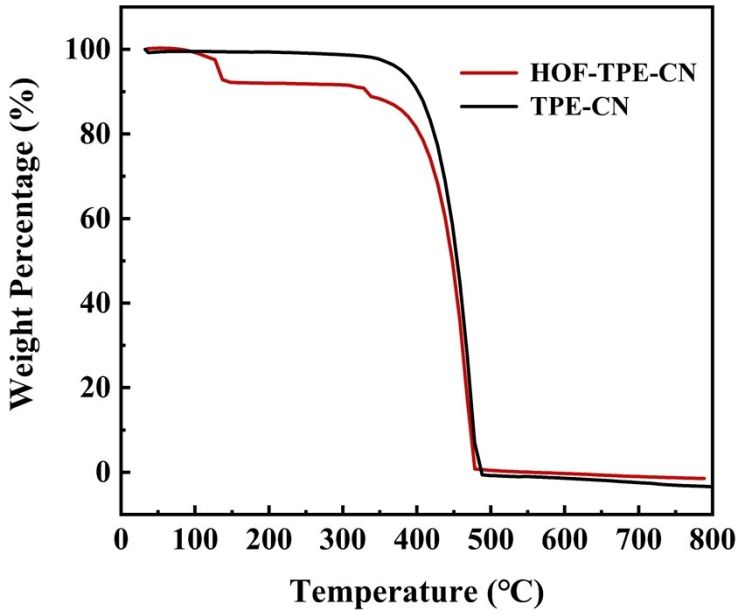

Fig. S4 TGA curve of TPE-CN and as-synthesized HOF-TPE-CN.

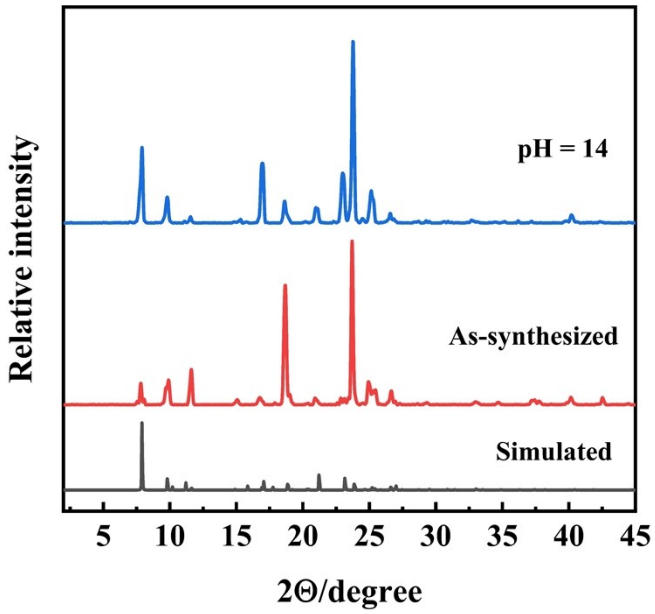

Fig. S5 PXRD patterns of as-synthesized HOF-TPE-CN and after immersed in pH = 14 NaOH solutions.

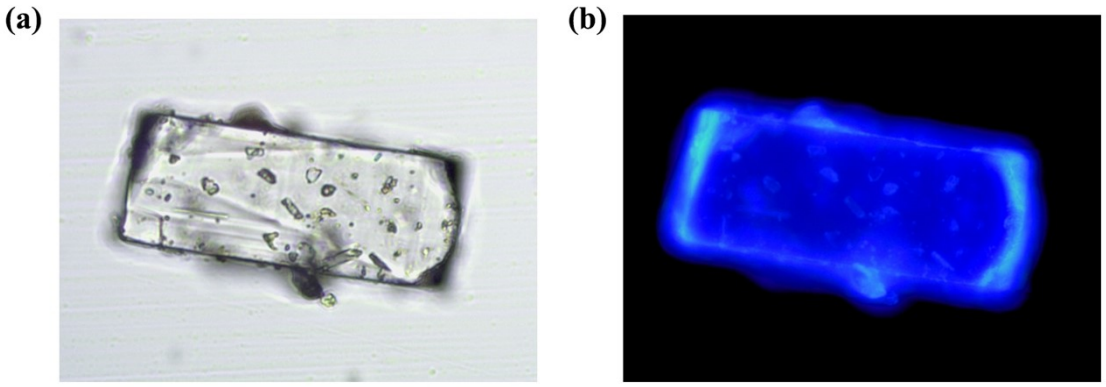

Fig. S6 The optical microscopy image of crystals after soaking into pH = 14 NaOH solutions under (a) bright field and (b) 365 nm excitation.

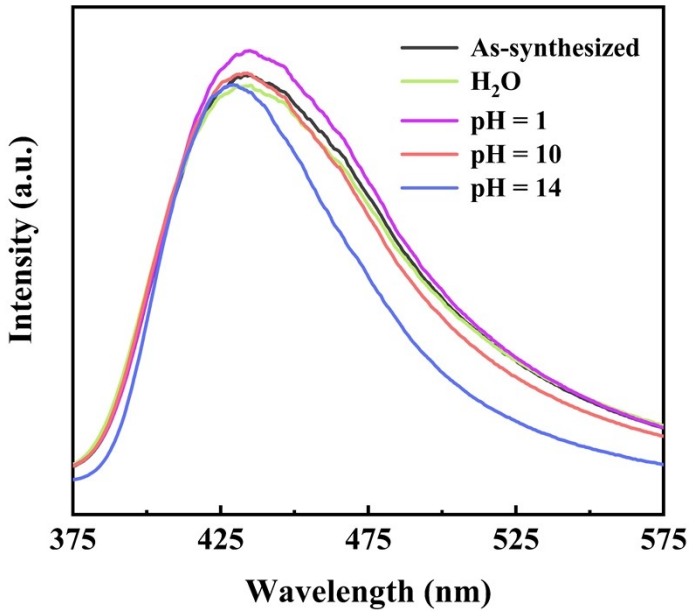

Fig. S7 Fluorescence spectra of HOF-TPE-CN after treatment with different pH aqueous solutions.

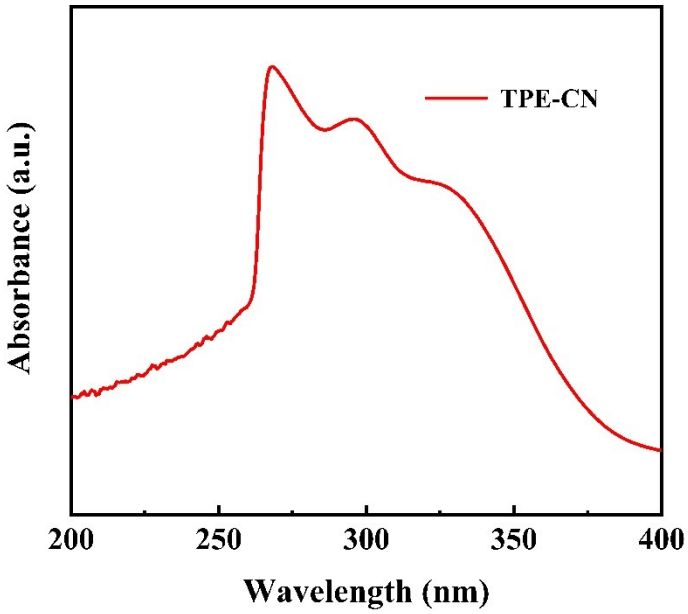

Fig. S8 UV-Vis spectrum of TPE-CN (10 μM) in DMF solution.

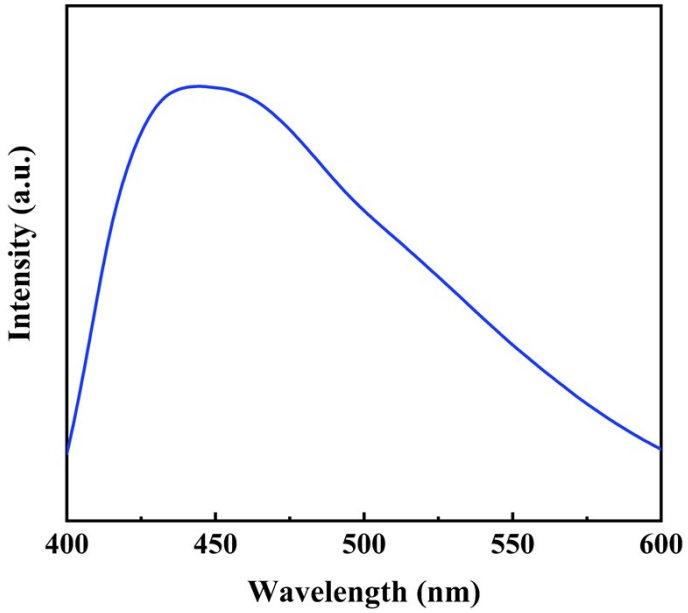

Fig. S9 Fluorescence emission spectra of a single crystal under the excitation of 365 nm.

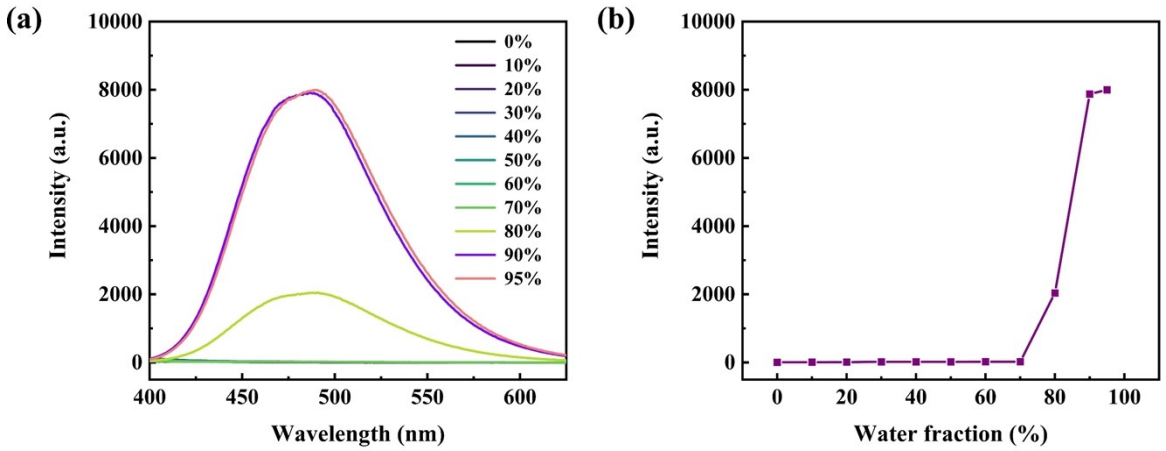

Fig. S10 (a) The fluorescence spectra of TPE-CN (10 μM) in acetone/H_2O mixtures with different H_2O fractions. (b) Changes of fluorescence intensity of TPE-CN in acetone/H_2O mixtures (λ = 490 nm) with different water fractions. λ_{ex} = 324 nm.

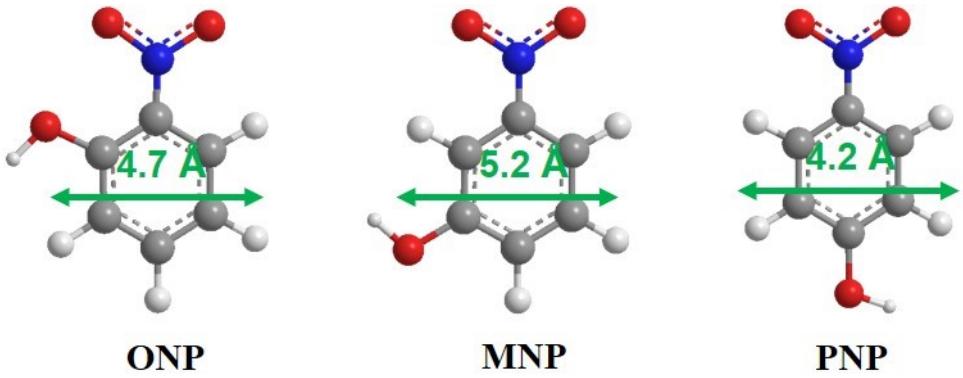

Fig. S11 The dimension of nitrophenol molecules.

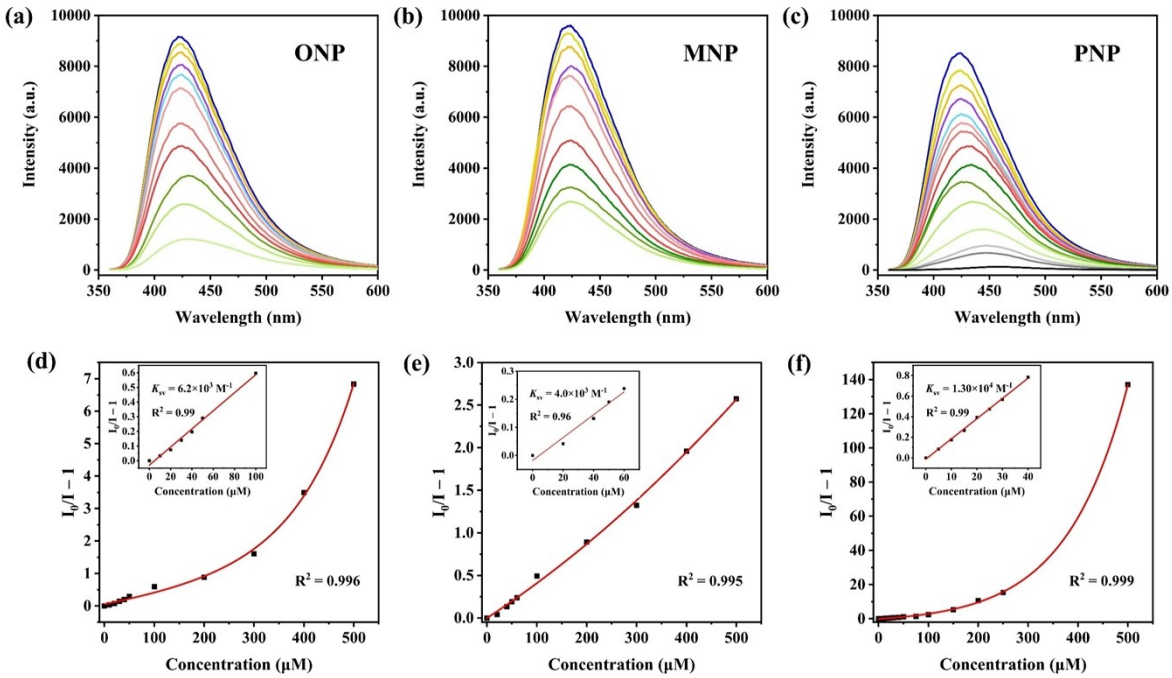

Fig. S12 Fluorescence spectra of HOF-TPE-CN dispersing in tap water (1 mg/mL) with the increasing concentrations (0–500 μM) of (a) ONP; (b) MNP; (c) PNP.

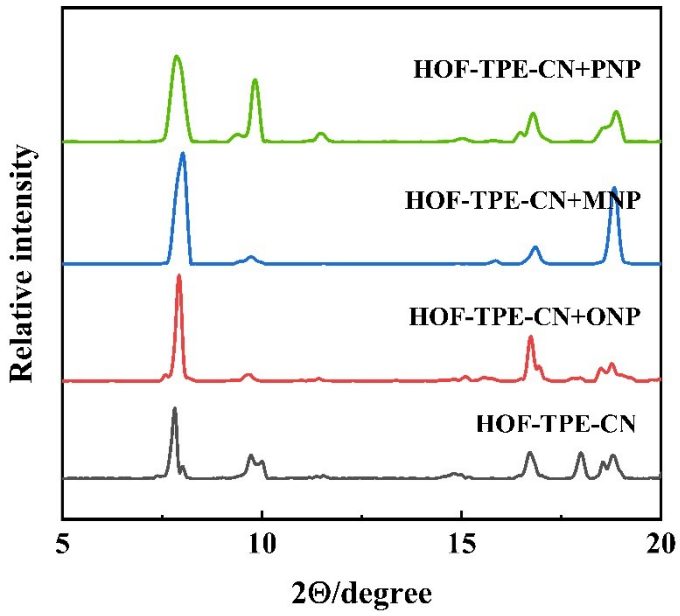

Fig. S13 PXRD patterns of HOF-TPE-CN and after immersed in nitrophenol solution ($1*10^{-2}$ M) for 2 days.

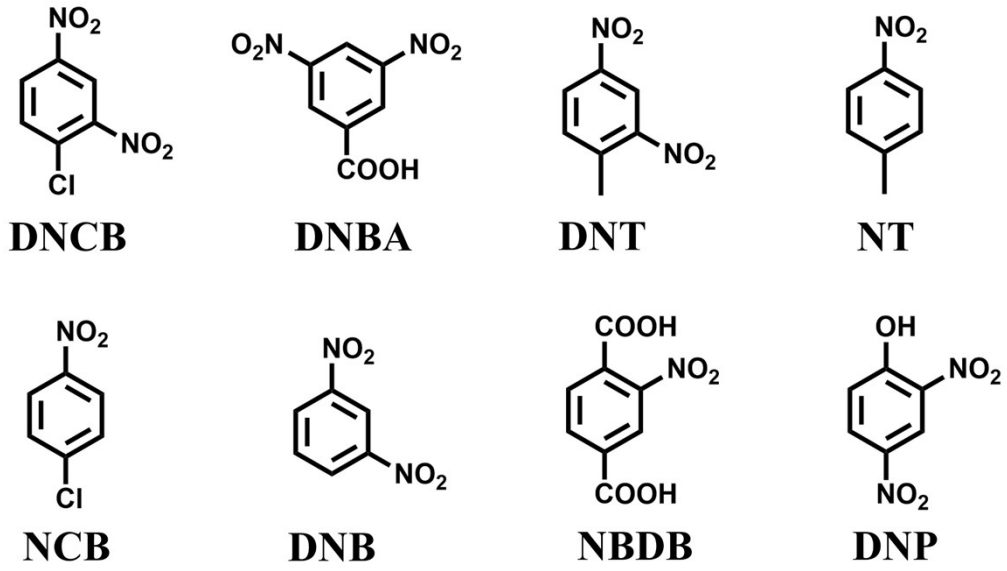

Fig. S14 Molecular structure and abbreviations of different nitroaromatic compounds.

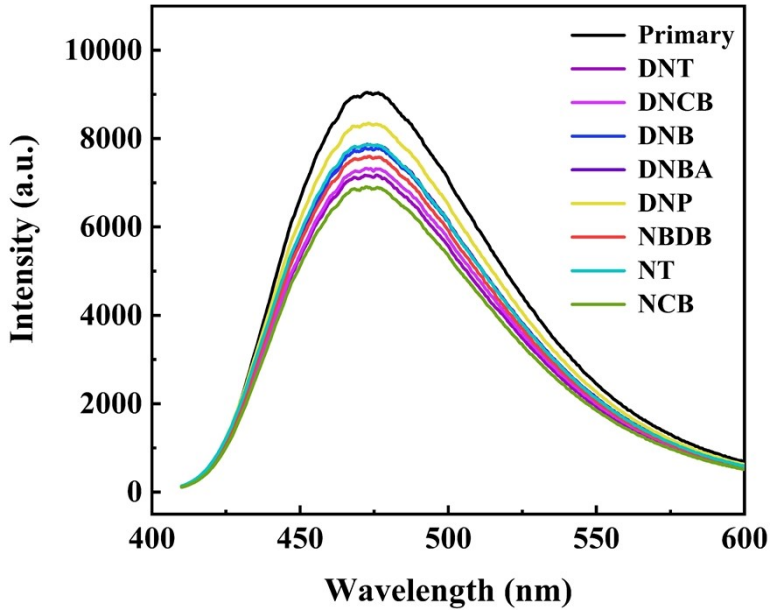

Fig. S15 The fluorescence spectra after adding different nitroaromatic compounds at the concentration of 500 μM.

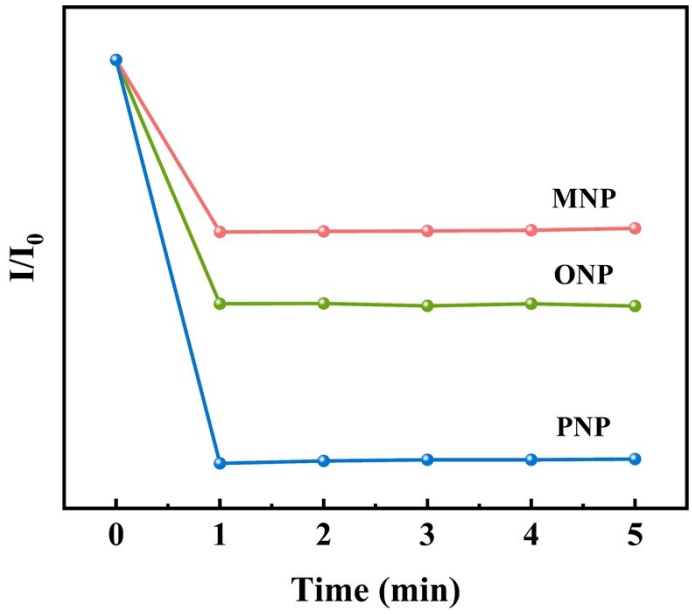

Fig. S16 The variation of fluorescence intensity of HOF-TPE-CN at 425 nm over time after the addition of nitrophenol (100 μM).

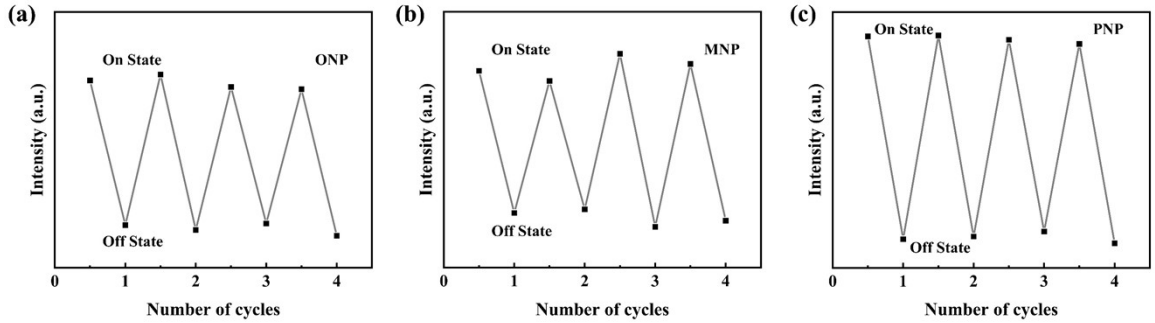

Fig. S17 Quenching and recovery test of HOF-TPE-CN toward (a) ONP, (b) MNP, and (c) PNP. The fluorescence intensity of HOF-TPE-CN suspension was recorded before and after adding the sample into 50 μM mono-nitrophenols, respectively. The HOF-TPE-CN samples were recovered by centrifugation and washed with H_2O solutions in several times. Then, the HOF-TPE-CN suspension was prepared with the same initial concentration for the next cycle.

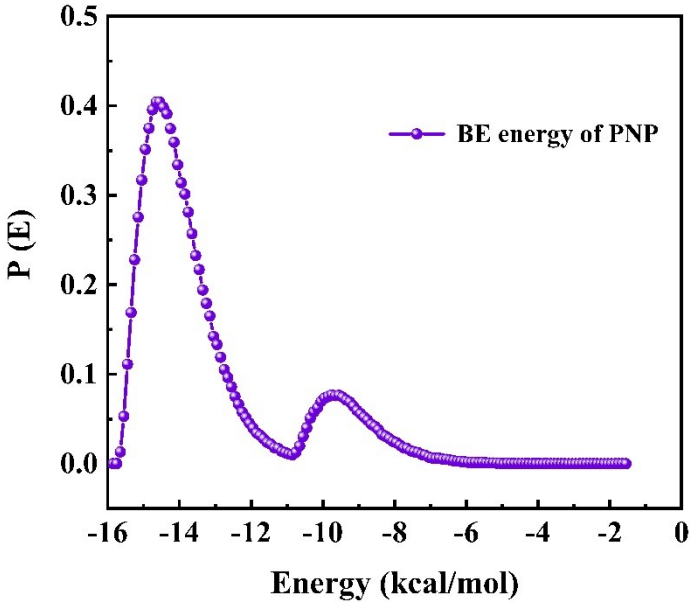

Fig. S18 CBMC molecular simulation: binding energy of PNP with HOF-TPE-CN.

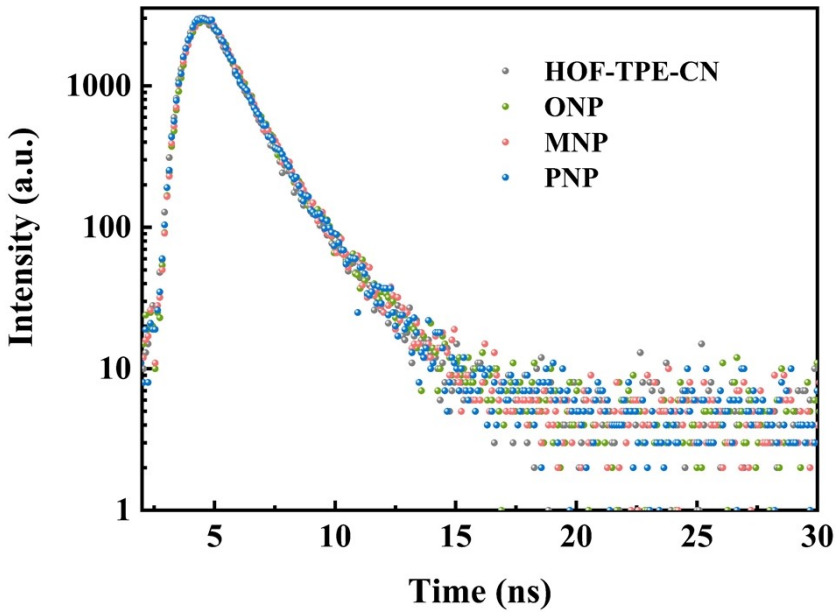

Fig. S19 The change of lifetime curves of HOF-TPE-CN at 420 nm before and after adding nitrophenol.

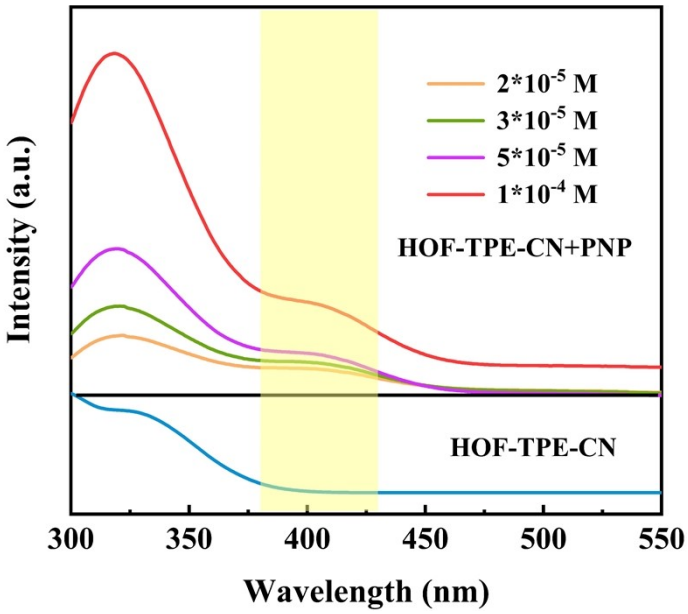

Fig. S20 UV-vis spectra of HOF-TPE-CN on incremental addition of PNP solution in water. As the gradual addition of PNP, a new peak appears in the UV-vis absorption spectrum of HOF-TPE-CN around 400 nm indicates the formation of stable ground-state charge transfer complexes

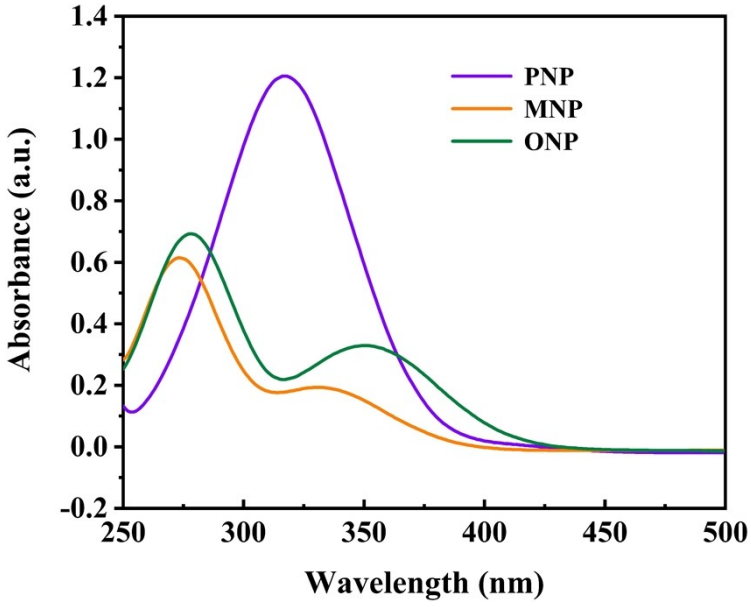

Fig. S21 UV-vis spectra of mono-nitrophenols in water.

Table S1 Crystallographic data and structure refinement results of HOF-TPE-CN.

Unit cell parameters	HOF-TPE-CN
Formula	$C_{30}H_{16}N_4$
Formula weight	432.47
Crystal system	tetragonal
Space group	$I4_1/acd$
a (Å)	22.3509
b (Å)	22.3509
c (Å)	20.7853
α (°)	90
β (°)	90
γ (°)	90
Cell volume (Å^3)	10383.56
Z	16
D_{calc} (g·cm^{-3})	1.1065
F(000)	3584.0
GOF	1.044

Table S2 Comparison of present work with some previous reports on the detection of mono-nitrophenol.

Material	Analytes	Medium systems	K_{sv} (M^{-1})	Limit of Detection (LOD)	Reference
$Zr_6O_4(OH)_8(H_2O)_4(CTTA)_{8/3}$	PNP	H_2O	4.2×10^4	NA	6
$Zr_6O_4(OH)_8(H_2O)_4(TTNA)_{8/3}$	PNP	H_2O	4.7×10^4	NA	6
$\{[Tb_2(L)_3(H_2O)_4]\cdot 10H_2O\}_n$	ONP	DMF	2.1×10^3	NA	7
	MNP	DMF	1.9×10^3	NA	
	PNP	DMF	4.9×10^3	NA	
$(pbpy)[Eu_2(NH_2BDC)_4(H_2O)]\cdot 3H_2O$	PNP	DMF/H_2O	2.52×10^3	9.52 μM	8
Th-TCBPE	ONP	H_2O		0.44 μM	9
	PNP	H_2O		0.7 μM	
CD@RCC3	ONP		75	NA	10
	MNP		24	NA	
	PNP		95	NA	
DL-COF	PNP	Ethanol	3.18×10^6	57.31 *n*M	11
$[Pb_7(TTPCA)_4Cl_2]\cdot 3H_2O$	ONP	DMA	7.6×10^3	7.09 μM	12
Pythz-COF,	PNP	Ethanol	4.4×10^4	24.9 μM	13
Pyaph-COF	PNP	Ethanol	2.6×10^4	42 μM	13
$[Zn_7(DPOT)_2(H_2O)_{11}]\cdot 2OH\cdot 3H_2O\cdot 5DMA$	PNP	Ethanol	5.78×10^4	4.77 μM	14
CHOF-1	PNP	Ethanol	NA	[1]8.78 μM	15
HOF-TPE-CN	ONP	H_2O	7×10^3	1.1 μM	This work
	MNP		3.5×10^3	2.39 μM	
	PNP		1.34×10^4	0.65 μM	

NA = not available

L = 5-(pyridine-4-ylmethoxy)isophthalic acid)

NH_2-BDC = 2-aminobenzene-1,4-dicarboxylic acid

H_6TDPAT = 2,4,6-tris(3,5-dicarboxylphenylamino)-1,3,5-triazine

H_3TTPCA = 1,1′,1″-(1,3,5-triazine-2,4,6-triyl)-tripiperidine-4-carboxylic acid]

H_6DPOT= 5,5’,5’’-((1,3,5-triazine-2,4,6-triyl)tris(oxy)) tri-isophthalic acid

References

1. T. Luo, P. Das, D. L. White, C. Liu, A. Star and N. L. Rosi, *J. Am. Chem. Soc.*, 2020, **142**, 2897–2904.
2. Z. Hu, W. P. Lustig, J. Zhang, C. Zheng, H. Wang, S. J. Teat, Q. Gong, N. D. Rudd and J. Li, *J. Am. Chem. Soc.*, 2015, **137**, 16209–16215.
3. Q. Huang, K. I. Otake and S. Kitagawa, *Angew. Chem., Int. Ed.*, 2023, **62**, e202310225.
4. X. Yu, A. A. Ryadun, D. I. Pavlov, T. Y. Guselnikova, A. S. Potapov and V. P. Fedin, *Angew. Chem., Int. Ed.*, 2023, **62**, e202306680.
5. L. J. Farrugia, *J. Appl. Cryst.*, 2012, **45**, 849–854.
6. B. Wang, X. Lv, D. Feng, L. Xie, J. Zhang, M. Li, Y. Xie, J. Li and H. Zhou, *J. Am. Chem. Soc.*, 2016, **138**, 6204–6216.
7. Z. Sun, P. Hu, Y. Ma and L. Li, *Dyes Pigment.*, 2017, **143**, 10–17.
8. H. S. Li, S. H. Xing, Y. Xiao, C. Wang, Q. L. Guan, F. Y. Bai, Y. H. Xing and F. Xu, *Chem. – Eur. J.*, 2023, **29**, e202202810.
9. Q. L. Guan, F. Xu, Y. Xiao, Z. X. You, F. Y. Bai and Y. H. Xing, *Adv. Mater. Interfaces*, 2022, **9**, 2201547.
10. Z. Lu, X. Lu, Y. Zhong, Y. Hu, G. Li and R. Zhang, *Anal. Chim. Acta*, 2019, **1050**, 146–153.
11. M. Faheem, S. Aziz, X. Jing, T. Ma, J. Du, F. Sun, Y. Tian and G. Zhu, *J. Mater. Chem. A*, 2019, **7**, 27148–27155.
12. S. Yu, K. Y. Zhang, J. X. Li, Y. Xiao, L. X. Sun, F. Y. Bai and Y. H. Xing, *Inorg. Chem.*, 2021, **60**, 7887–7899.
13. S. Jiang, L. Meng, M. Lv, F. Bai, W. Tian and Y. Xing, *Microporous Mesoporous Mat.*, 2023, **348**, 112408.
14. M. Liu, M. Y. Wang, R. Huo, C. Wang, Y. H. Xing, F. Y. Bai and F. Xu, *J. Mater. Chem. C*, 2022, **10**, 11676–11685.
15. C. Zhang, F. Sun and Y. He, *ACS Appl. Mater. Interfaces*, 2023, **15**, 9970–9977.